Ultra-Strong Light-Matter Coupling in Deeply Subwavelength THz LC resonators Supplementary Information

Mathieu Jeannin,*,† Giacomo Mariotti Nesurini,† Stéphan Suffit,† Damal Gacemi,† Angela Vasanelli,† Lianhe Li,‡ Alexander Giles Davies,‡ Edmund Linfield,‡ Carlo Sirtori,† and Yanko Todorov†

†*Laboratoir Matériaux et Phénomènes Quantiques, Université Paris Diderot, Sorbonne Paris Cité, CNRS-UMS 7162, 75013 Paris, France*

‡*School of Electronic and Electrical Engineering, University of Leeds, LS2 9JT Leeds, United Kingdom*

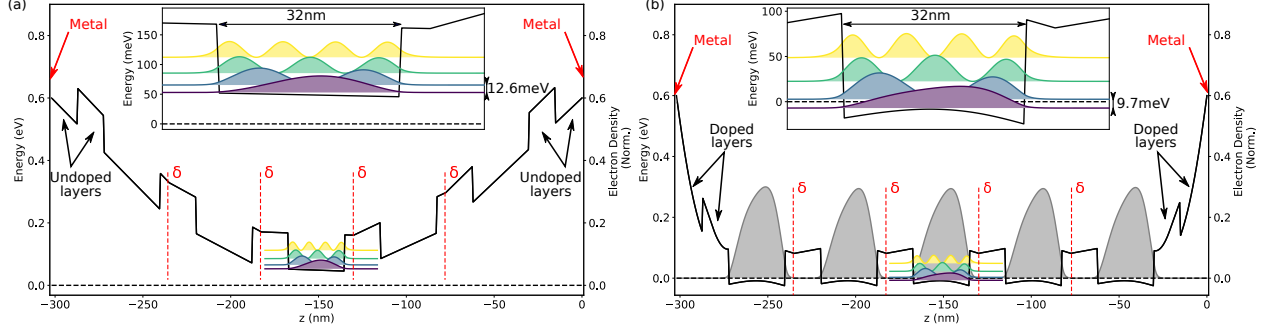E-mail: mathieu.jeannin@univ-paris-diderot.fr

Contents

Figure S1: Simulated band structures for a 5 QW sample showing the conduction band profile bending assuming a 0.6 V Schottky barrier at each metal-semiconductor interface for undoped outermost layers (a), and the ideal doping of the outermost layers (b). In (a), the whole structure is depleted. The electron density is represented in grey in (b). Inset: Electron wave function (squared modulus) in the central QW. The Fermi energy is represented in dashed line. The Siδ-doping layers are represented in red dashes.

S1   Band Structure

The sample design has to take into account the conduction band profile bending at the metal-semiconductor interface. In order to estimate this effect, we use a freely available Schrödinger-Poisson solver[1] to solve for the band profile self-consistently, coupled to an in-house Schrödinger solver accounting for non-parabolicity. We assume a 0.6 V barrier at the Au-GaAs interface. If no special care is taken for the outermost layers of the structure, as in Fig. S1 (a), the Schottky barrier leads to a rise of the conduction band edge, fully depleting the structure. To compensate for this effect, the outermost GaAs and Al$_{0.15}$Ga$_{0.85}$As layers must be doped. The targeted band profile is shown in Fig. S1 (b). In real structures, the actual dopant concentration is unknown and requires careful empirical tuning and calibration to achieve an optimal result. Moreover, the exact barrier height is also unknown an depends on the GaAs surface defect density. We show in the main text that our first sample was too lightly doped at the metal-semiconductor interfaces, while the second one suffered from free carrier absorption caused by electrons in the outermost GaAs layers.

S2   Lumped elements model

The resonant frequency of the LC resonator is evaluated using a lumped element model, following previous work on structure without QWs.[2] The capacitance of the structure is calculated using the formula for two parallel strip lines, which allows accounting for the parasitic capacitance between the two arms of the resonator.[3] The formula for an odd-mode coupling is:

$$C = C_f + C_p + C_{gd} + C_{ga} \qquad (1)$$

where C_p is the usual planar capacitance between the strip and the ground plane, C_f is the fringing field capacitance at the outer edge of the strip only. C_{ga} and C_{gd} are the gap capacitance between the two microstrip lines respectively in air and the dielectric substrate.

The exact expression of C_{ga} involves the ratio of the elliptic function and its complement, which can be approximated as:

$$k = \frac{S}{S + 2W}, \qquad k' = \sqrt{1 - k^2} \tag{2}$$

$$C_{ga} = \begin{cases} \frac{\varepsilon_0}{\pi} \ln\left(2\frac{1+\sqrt{k'}}{1-\sqrt{k'}}\right), & 0 \leq k^2 \leq 0.5 \\ \frac{\varepsilon_0 \pi}{\ln\left(2\frac{1+\sqrt{k}}{1-\sqrt{k}}\right)}, & 0.5 \leq k^2 \leq 1 \end{cases} \tag{3}$$

where W is the width of the strip and S the length of the gap between the strips (L_x in the main text). The C_{gd} capacitance is:

$$C_{gd} = \frac{\varepsilon_0 \varepsilon}{\pi} \ln\left(\coth\left(\frac{\pi S}{4d}\right)\right) + 0.65 C_f \left(\frac{0.02d}{S}\sqrt{\varepsilon} + \left(1 - \frac{1}{\varepsilon^2}\right)\right) \tag{4}$$

where d is the capacitor thickness, and ε the permittivity of the embedding dielectric material (SiN in our case). Similarly, we calculate the total inductance by summing all the individual inductances of each straight wire of the inductive loop and of the connecting wire on the ground pad, and all the mutual inductances between parallel wires. The inductance of a thin wire is given by:[4]

$$L = 2l \left(\ln\left(2l/r\right) - 1\right) \tag{5}$$

while the mutual inductance between two parallel wires is:[4]

$$M_{i\|j} = 0.001 \left[z \ln\left(z + \sqrt{z^2 + \rho^2}\right) - \sqrt{z^2 + \rho^2}\right]_{l_2+l_3-l_1,l_3}^{l_3-l_1,l_3+l_2} (z) \tag{6}$$

where l_1 is the length of the first wire, l_2 is the length of the second wire, l_3 is the signed distance between the first end of each wire, and ρ their parallel separation, and

$$\left[f(z)\right]_{s_2,s_4}^{s_1,s_3} (z) = \sum_{k=1}^{4} (-1)^{k+1} f(s_k) \tag{7}$$

The value of M is in μH for lengths in centimetres. Finally, the total inductance reads:[3]

$$L_{tot} = \sum_i L_i - 2 \sum_{i\|j} M_{ij} \tag{8}$$

The resonant frequency is ultimately given by $f = 1/2\pi\sqrt{LC}$.

S3   25 QWs reference sample

We present in Fig. S2 the properties of the 25 QWs reference sample processed into patch cavities. Fig. S2 (a) shows the reflectivity of the 13μm patch as a function of temperature, showing a clear polaritonic splitting as the temperature decreases. Fig. S2 (b) shows the
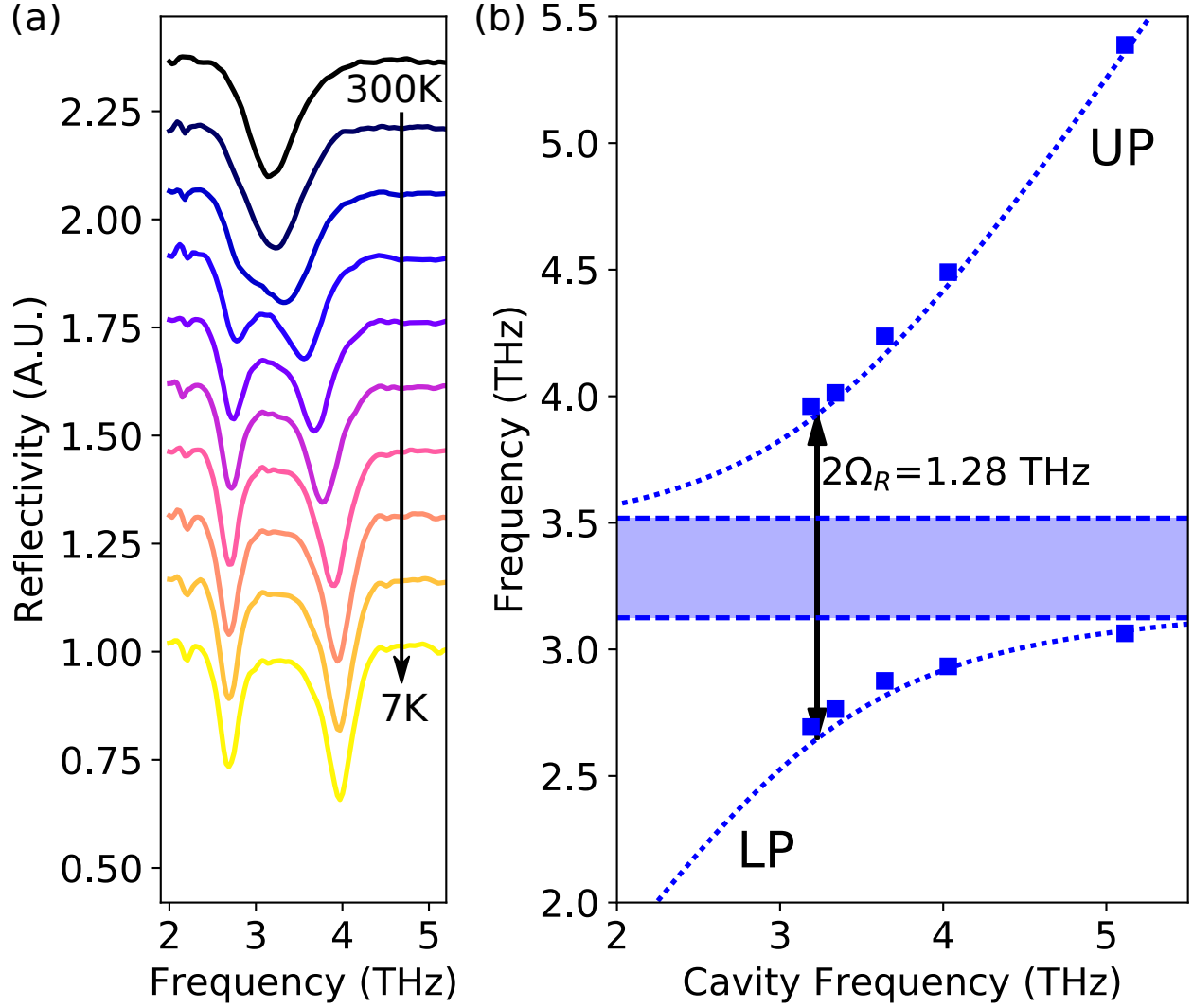
Figure S2: 25 QW sample processed into patch microcavities. Left: reflectivity as a function of temperature for the cavity closest to the matter resonance. Right: polariton dispersion relation as a function of cavity frequency. The Rabi splitting is $2\Omega_R = 1.28$ THz$= 0.4\tilde{\omega}$.

dispersion relation of the two polaritonic branches, allowing us to determine the intersubband plasmon frequency $\tilde{\omega} = 3.6$ THz and the Rabi splitting $2\Omega_R = 1.28$ THz. We recall here equation (2) of the main text, which is the basis of our analysis:

$$2\Omega_R = \sqrt{\Psi^2 f_w f_{12}} \omega_P = \sqrt{\frac{\Psi^2 f_{12} e^2 N_{QW}(n_1 - n_2)}{\varepsilon\varepsilon_0 m^* d}} \tag{9}$$

From the knowledge of the polariton splitting alone, one can only deduce the product $\Psi f_{12} N_{QW}(n_1 - n_2)$. Assuming that at low enough temperature, $n_2 = 0$, and furthermore that $\Psi \approx 1$ for the patch cavities, we can determine the product

$$f_{12} N_{QW} n_1 = (2\Omega_R/e)^2 \varepsilon\varepsilon_0 m^* d = 22 \times 10^{11} \text{cm}^{-2} \tag{10}$$

Using a Schrödinger-Poisson solver, and making successive hypothesis on the (integer) number of populated quantum wells, we can determine the doping in each quantum well and the corresponding oscillator strength. It is important to note that the oscillator strength and the doping density have a complex interplay on the Rabi frequency, as a larger doping density increases the Rabi frequency through the n_1 term, but lowers the oscillator strength f_{12} as it deforms the QW and hence changes the overlap between the electron wave functions. The resulting doping density can be checked by calculating the theoretical value of the intersubband plasmon frequency $\tilde{\omega} = \sqrt{\omega_{12}^2 + \omega_P^2}$ from the plasma frequency. This theoretical value can be compared to the experimental determination of $\tilde{\omega}$, which is determined as the asymptotic value of the upper polariton branch as the cavity frequency tends towards zero.

As an example, in the case of the 25 QWs sample, we find that 21 QWs are populated, resulting in a surface equivalent doping per quantum well of $n_1 = 1.37 \times 10^{11} \text{cm}^{-2}$, and an oscillator strength $f_{12} = 0.907$. Note that this value differs from the ideal quantum well one of $f_{12-ideal} = 0.96$. These values will be the starting point of our data analysis procedure, discussed below, to determine the properties of the 5 QWs samples processed into patch cavities and LC resonators.

S4   Iterative procedure for the data analysis

We describe here the iterative procedure used to determine the electron density in each sample. Starting with the first 5 QWs sample in the main text (sample A hereafter) processed into patch cavities, and comparing the Rabi splitting with the one of the 25 QWs sample, we get:

$$\left(\frac{\Omega_R^A}{\Omega_R^{25}}\right)^2 = \frac{f_{12}^A N_{QW}^A n_1^A}{f_{12}^{25} N_{QW}^{25} n_1^{25}} \tag{11}$$

where the denominator on the right hand side has been determined in the previous section.

From the Rabi splitting deduced in Fig. 4 (a) of the main text, $\Omega_R^A = 0.85$ THz, we obtain the product $f_{12}^A N_{QW}^A n_1^A = 2.5 \times 10^{11} \text{cm}^{-2}$. Assuming that the surface charge density is equal in both samples, e.g. $n_1^A = n_1^{25} = 1.37 \times 10^{11} \text{cm}^{-2}$, we have the same oscillator strength $f_{12}^A = 0.907$ and we get $N_{QW}^A = 2$. These hypothesis are further confirmed by calculating the intersubband plasmon frequency $\tilde{\omega} = 3.56$ THz, in very good agreement with the results

presented in Fig. 4 (a) of the main text.

We can then make use of this result to characterize the LC resonators processed on the same 5 QWs sample, using the patch cavities as a reference, assuming that the number of populated QWs is the same:

$$\left(\frac{\Omega_R^{A-LC}}{\Omega_R^{A-patch}}\right)^2 = \frac{\Psi_{A-LC}^2 f_{12}^{A-LC} n_1^{A-LC}}{\Psi_{A-patch}^2 f_{12}^{A-patch} n_1^{A-patch}} \tag{12}$$

If we naively assume in a first step that the electronic population is strictly the same, the ratio of the Rabi frequencies directly yields the optical confinement factor:

$$\frac{\Omega_R^{A-LC}}{\Omega_R^{A-patch}} = \Psi_{A-LC} = 0.84 \tag{13}$$

since $\Psi_{A-patchs} \approx 1$. However, Fig. 4 in the main text clearly evidences that the patch cavities and LC resonators have different intersubband plasmon frequencies $\tilde{\omega}$, indicating a different doping density. An iterative procedure using Schrödinger-Poisson simulations should thus be employed to well encompass the interplay between the oscillator strength and the doping density in the Rabi frequency. A doping density of $n_1 = 1.2 \times 10^{11}\mathrm{cm}^{-2}$ yields an oscillator strength of $f_{12}^{LC} = 0.918$, and the correct ISB plasmon frequency $\tilde{\omega} = 3.5$ THz. We can thus correct the confinement factor which ultimately reads $\Psi_{A-LC} = 0.89$. Finally, using the number of populated QWs and the surface equivalent doping per QW, we get that $N_{e-patchs}^A = 3.3 \times 10^5 \mathrm{e}^-/\text{patch}$ and $N_{e-LC}^A = 2.4 \times 10^3 \mathrm{e}^-/\text{capacitor}$.

For the sake of consistency, we can try to relax the assumption $N_{QW}^{A-LC} = N_{QW}^{patch} = 2$. As the product $f_{12}N_{QW}n_1$ has to be conserved, using $N_{QW}^{A-LC} = 1$ results in a doping density of around $n_1 = 2 \times 10^{11}\mathrm{cm}^{-2}$, $f_{12} = 0.87$ and $\tilde{\omega} = 3.76$ THz, which is larger than the measured value. Inversely, $N_{QW}^{A-LC} = 3$ results in a doping density of around $n_1 = 0.8 \times 10^{11}\mathrm{cm}^{-2}$, $f_{12} = 0.936$ and $\tilde{\omega} = 3.35$ THz, which is lower than the measured value. These values are shown in stars in Fig. 4 (b) of the main text. We can thus confirm the values determined above.

S5 5 QWs, increased doping (sample B)

We present in Fig. S3 the properties of the 5 QWs sample with increased doping (hereafter designated as sample B), processed into patch cavities (Fig. S3 (a)), and compared to the LC resonators (Fig. S3 (b)). From the dispersion relation of the sample processed into patch cavities (Fig. S2 (a))we determine the intersubband plasmon frequency $\tilde{\omega} = 3.6$ THz and the Rabi splitting $2\Omega_R = 1.28$ THz.

Using the same iterative procedure, we can deduce the product $f_{12}^{B-patch} N_{QW}^{B-patch} n_1^{B-patch}$ in the new sample by comparing the Rabi splitting with the previous 5 QWs sample, and accounting for the thickness difference between the active regions:

$$f_{12}^{B-patch} N_{QW}^{B-patch} n_1^{B-patch} = f_{12}^{A-patch} N_{QW}^{A-patch} n_1^{A-patch} \frac{d^{B-patch}}{d^{A-patch}} \left(\frac{\Omega_R^{B-patch}}{\Omega_R^{A-patch}}\right)^2 \tag{14}$$
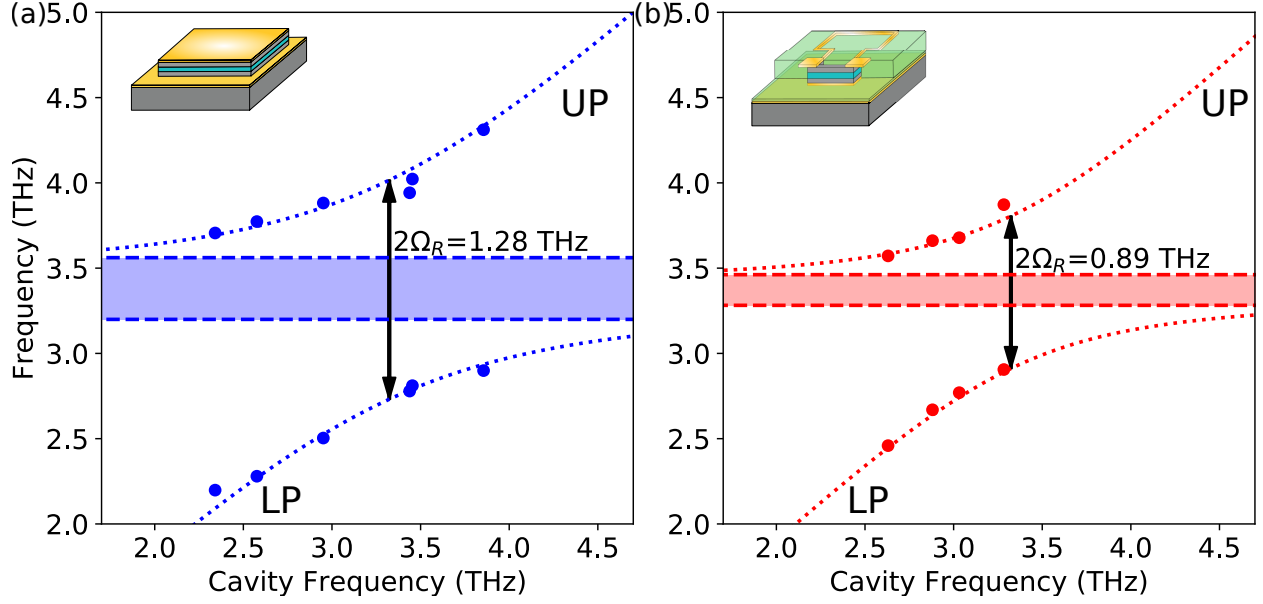
Figure S3: Polariton dispersion relation in the case of patch microcavities (left) and LC resonators (right) for the sample with the largest doping in the outer GaAs layers.

which yields $f_{12}^{B-patch} N_{QW}^{B-patch} n_1^{B-patch} = 6.26 \times 10^{11} \text{cm}^{-2}$. Using Schrödinger-Poisson simulations, we obtain a doping density of $n_1^{B-patch} = 1.4 \times 10^{11} \text{cm}^{-2}$ and a number of populated QWs $N_{QW}^{B-patch} = 5$.

We can then use these values to characterize the LC resonators fabricated on the same sample. Again, we can check that the number of populated QWs is the same, $N_{QW}^{B-LC} = 5$. Using Schrödinger-Poisson simulations, we obtain a doping density of $n_1^{B-LC} = 1.2 \times 10^{11} \text{cm}^{-2}$ and a corresponding oscillator strength $f_{12}^{B-LC} = 0.918$. Applying the same equality as equation (12) on sample B, we finally get $\Psi_{B-LC} = 0.75$. We finally calculate that in this sample, $N_{e-patch}^B = 8.5 \times 10^5 \text{e}^-/\text{patch}$ and $N_{e-LC}^B = 6 \times 10^3 \text{e}^-/\text{capacitor}$.

References

(1) Tan, I.-H.; Snider, G. L.; Chang, L. D.; Hu, E. L. A Self-consistent Solution of Schrödinger–Poisson Equations Using a Nonuniform Mesh. *Journal of Applied Physics* **1990**, *68*, 4071–4076.

(2) Todorov, Y.; Desfonds, P.; Belacel, C.; Becerra, L.; Sirtori, C. Three-Dimensional THz Lumped-Circuit Resonators. *Optics Express* **2015**, *23*, 16838.

(3) Bahl, I. J. *Lumped Elements for RF and Microwave Circuits*; Artech House Microwave Library; Artech House: Boston, Mass., 2003; OCLC: 248963480.

(4) Hoer, C.; Love, C. Exact Inductance Equations for Rectangular Conductors with Applications to More Complicated Geometries. *Journal of Research of the national bureau of standards - C.* **1965**, *69C*, 127.